Special issue research article

NMR IN BIOMEDICINE

Received: 24 December 2015, Revised: 23 June 2016, Accepted: 17 August 2016, Published online in Wiley Online Library: 12 October 2016

(wileyonlinelibrary.com) DOI: 10.1002/nbm.3628

Heterogeneous anisotropic magnetic susceptibility of the myelin-water layers causes local magnetic field perturbations in axons†

Steffan Puwal[a], Bradley J. Roth[a] and Peter J. Basser[b]*

One goal of MRI is to determine the myelin water fraction in neural tissue. One approach is to measure the reduction in T_2* arising from microscopic perturbations in the magnetic field caused by heterogeneities in the magnetic susceptibility of myelin. In this paper, analytic expressions for the induced magnetic field distribution are derived within and around an axon, assuming that the myelin susceptibility is anisotropic. Previous models considered the susceptibility to be piecewise continuous, whereas this model considers a sinusoidally varying susceptibility. Many conclusions are common in both models. When the magnetic field is applied perpendicular to the axon, the magnetic field in the intraaxonal space is uniformly perturbed, the magnetic field in the myelin sheath oscillates between the lipid and water layers, and the magnetic field in the extracellular space just outside the myelin sheath is heterogeneous. These field heterogeneities cause the spins to dephase, shortening T_2*. When the magnetic field is applied along the axon, the field is homogeneous within water-filled regions, including between lipid layers. Therefore the spins do not dephase and the magnetic susceptibility has no effect on T_2*. Generally, the response of an axon is given as the superposition of these two contributions. The sinusoidal model uses a different set of approximations compared with the piecewise model, so their common predictions indicate that the models are not too sensitive to the details of the myelin-water distribution. Other predictions, such as the sensitivity to water diffusion between myelin and water layers, may highlight differences between the two approaches. Copyright © 2016 John Wiley & Sons, Ltd.

Keywords: MRI; myelin; susceptibility; anisotropic; myelin water imaging; perturbation

INTRODUCTION

Magnetic resonance imaging has been used to monitor the fraction of water trapped between myelin layers of neural tissue (1–4). This technique has been applied to diagnose diseases such as multiple sclerosis (5), spinal cord injury (6), and autism (7), and to study brain development (8,9). Typically, multicomponent analysis predicts the distribution of T_1, T_2, and T_2* in different water pools. Free water has a relatively long T_2*, and myelin water trapped between layers of the myelin sheath has a relatively short T_2*. The relative fraction of water within the myelin indicates the degree of myelination and integrity of the axons and possibly could serve as an imaging biomarker to assess normal and abnormal development, dysmyelination, or demyelination.

One hypothesis is that T_2* relaxation arises from microscopic perturbations in the magnetic field, causing spins to dephase. A heterogeneous distribution of magnetic susceptibility could cause such perturbations. Interest in magnetic susceptibility imaging is growing (10,11), and it is now an important contrast mechanism in magnetic resonance imaging (12–17), particularly for studying the white matter in the brain (15,18–26).

To determine the magnetic field caused by a heterogeneous susceptibility distribution in and around an axon, we must solve a partial differential equation obtained from the static limit of Maxwell's equations. Previously, we analyzed this problem for isotropic myelin susceptibility (27). In this paper, we extend the analysis in Reference 27 to consider anisotropic myelin susceptibility (18). We calculate the resulting induced magnetic field distribution and estimate how this field will affect T_2*, including the prediction of its orientational dependence.

Our model assumes a sinusoidal oscillation of the magnetic susceptibility within the myelin sheath. Previous models have assumed a piecewise constant oscillation (21). We believe that having two models for this system is valuable, because by comparing results we gain insight into which aspects of the model are robust to assumptions about the details of the myelin microstructure. One advantage of our model is that, although the physical model is approximate, the equations governing

* *Correspondence to: P. J. Basser, Eunice Kennedy Shriver National Institute of Child Health and Human Development, National Institutes of Health, Bethesda, MD, USA.*
E-mail: pjbasser@helix.nih.gov

a *S. Puwal, B. J. Roth*
Department of Physics, Oakland University, Rochester, MI, USA

b *P. J. Basser*
Eunice Kennedy Shriver National Institute of Child Health and Human Development, National Institutes of Health, Bethesda, MD, USA

† *This article has been contributed to by US Government employees and their work is in the public domain in the USA*

Abbreviations used: *μ_0, magnetic permeability; a, inner radius of myelin sheath; b, outer radius of myelin sheath; χ, magnetic susceptibility; k, wave number characterizing myelin-water layer thickness;* ***H****, magnetic field intensity;* ***B****, magnetic flux density.*

the magnetic field distribution can be solved analytically, yielding a closed-form solution.

MODEL

We model an axon as an infinitely long, straight cylinder and indicate position with cylindrical coordinates (r, θ, z). The core of the cylinder $r < a$ represents the intracellular space (mostly water) with magnetic permeability μ_0.[1] Outside the cylinder, $r > b$, is the surrounding extracellular space, also with permeability μ_0. The myelin sheath, $a < r < b$, consists of alternating layers of myelin and water. We represent this structure by an oscillating magnetic permeability

$$\mu_r = \mu_0\left[1 + \frac{\chi}{2}(1 - \cos(k(r-a)))\right], \quad [1]$$

$$\mu_{\theta,z} = \mu_0\left[1 + w\frac{\chi}{2}(1 - \cos(k(r-a)))\right], \quad [2]$$

where μ_r is the permeability of the myelin in the radial (r) direction (along the fatty acid chains in the lipid molecules), $\mu_{\theta,z}$ is the permeability of the myelin in the θ and z directions (perpendicular to the fatty acid chains), and k is the spatial frequency corresponding to the individual layers of myelin making up the sheath. The myelin corresponds to $\cos(k(r-a)) = -1$, so χ is the magnetic susceptibility of the myelin in the radial direction, and w is a measure of its anisotropy ($w = 1$ corresponds to isotropy). The aqueous space between myelin layers corresponds to $\cos(k(r-a)) = 1$, so its permeability is isotropic and equal to that of the intracellular and extracellular spaces. The permeability is continuous at $r = b$ if we require that $k(b-a) = 2\pi n$, where n is the number of layers of myelin. The susceptibility χ is a dimensionless number with a magnitude of about 10^{-5} in biological tissue. Most biological tissues are diamagnetic, so χ is negative. In lipids, the susceptibility is larger in magnitude along the fatty acid chains than across them (21,28), implying that in our model w is less than unity.

No free current is present, so the curl of the magnetic H-field is zero, $\nabla \times \boldsymbol{H} = 0$, and we can write $\mathbf{H}$ in terms of a scalar magnetic potential, $\boldsymbol{H} = -\nabla\Phi$ (29). The magnetic field, $\mathbf{B}$, is related to $\mathbf{H}$ by $B_r = \mu_r H_r$, $B_\theta = \mu_\theta H_\theta$, and $B_z = \mu_z H_z$. Because the magnetic field has zero divergence ($\nabla \cdot \boldsymbol{B} = 0$) and the permeability varies only in the r direction, the differential equation we solve is

$$\frac{1}{r}\frac{\partial}{\partial r}\left(\mu_r r\frac{\partial\Phi}{\partial r}\right) + \mu_\theta\frac{1}{r^2}\frac{\partial^2\Phi}{\partial\theta^2} + \mu_z\frac{\partial^2\Phi}{\partial z^2} = 0. \quad [3]$$

Assuming that the magnetic field does not change in the z direction along the axon's axis, Eq. [3] simplifies to

$$\frac{\partial\mu_r}{\partial r}\frac{\partial\Phi}{\partial r} + \left[\mu_r\frac{1}{r}\frac{\partial}{\partial r}\left(r\frac{\partial\Phi}{\partial r}\right) + \mu_\theta\frac{1}{r^2}\frac{\partial^2\Phi}{\partial\theta^2}\right] = 0. \quad [4]$$

Our goal is to find the Φ that obeys Eq. [4] and results in a magnetic field that is continuous, implying that Φ and its radial derivative should be continuous at $r = a$ and b. $\mathbf{B}$ should be equal to the magnetic field $\mathbf{B}_0$ in the surrounding extracellular space when $r \gg b$.

RESULTS

Case 1. The applied magnetic field is perpendicular to the axon

If the magnetic field is applied in the x-direction ($\mathbf{B}_0 = B_0\mathbf{i}$), then far from the axon Φ approaches $-\frac{B_o}{\mu_o}r\cos\theta$. To find an analytical solution, we assume that the scalar magnetic potential has the form

$$\Phi(r) = -\frac{B_o}{\mu_o}r\left(1 + \chi\frac{g(r)}{r}\right)\cos\theta. \quad [5]$$

We then insert Eqs. [1], [2], and [5] into Eq. [4], ignoring terms in χ^2 (which will be small), and find

$$\frac{1}{r}\frac{d}{dr}\left(r\frac{dg(r)}{dr}\right) - \frac{g(r)}{r^2} = -\frac{1}{2}\left[k\sin(k(r-a)) + (1-w)\frac{1-\cos(k(r-a))}{r}\right] \quad [6]$$

in the myelin ($a < r < b$) and $\frac{1}{r}\frac{d}{dr}\left(r\frac{dg(r)}{dr}\right) - \frac{g(r)}{r^2} = 0$ elsewhere. The solution is

$$g(r) = A_1 r \qquad r < a \quad [7]$$

$$g(r) = A_2 r + \frac{A_3}{r} + \frac{1}{4}\left\{(1+w)\left[\frac{\sin(k(r-a))}{k} + \frac{\cos(k(r-a))}{k^2 r}\right] - (1-w)\left[r\ln\left(\frac{r}{a}\right) + r\cos(ka)\mathrm{Ci}(kr) - r\sin(ka)\mathrm{Si}(kr)\right]\right\} \qquad a < r < b \quad [8]$$

$$g(r) = \frac{A_4}{r} \qquad r > b. \quad [9]$$

The functions $\mathrm{Si}(x)$ and $\mathrm{Ci}(x)$ are the sine and cosine integrals (30)

$$\mathrm{Si}(x) = \int_0^x \frac{\sin u}{u}du \text{ and } \mathrm{Ci}(x) = \int_x^\infty \frac{\cos u}{u}du, \quad [10]$$

which obey

$$\frac{d\mathrm{Si}(x)}{dx} = \frac{\sin(x)}{x} \text{ and } \frac{d\mathrm{Ci}(x)}{dx} = -\frac{\cos(x)}{x}. \quad [11]$$

To determine the constants A_1, A_2, A_3, and A_4, we require that $g(r)$ and $dg(r)/dr$ are continuous at $r = a$ and b

[1] Although we assign the water-filled intracellular and extracellular spaces a permeability of μ_0 (zero susceptibility), this is not a limitation of the model. We could instead assign water any permeability and then take the susceptibility χ in our model to be the difference between the water and myelin susceptibilities, and we would obtain the same result.

$$A_1 = \frac{1}{8}2(1-w)\left[\ln\left(\frac{b}{a}\right) - \cos(ka)(\mathrm{Ci}(ka) - \mathrm{Ci}(kb)) + \sin(ka)(\mathrm{Si}(ka) - \mathrm{Si}(kb))\right] \quad [12]$$

$$A_2 = \frac{1}{8}\left\{-(1+w) + 2(1-w)\left[\ln\left(\frac{b}{a}\right) + \cos(ka)\mathrm{Ci}(kb) - \sin(ka)\mathrm{Si}(kb)\right]\right\} \quad [13]$$

$$A_3 = \frac{1}{8}(1+w)\left(a^2 - \frac{2}{k^2}\right) \quad [14]$$

$$A_4 = -\frac{1}{8}(1+w)\left(b^2 - a^2\right). \quad [15]$$

If $w = 1$, the myelin is isotropic and the solution matches the one we derived previously for the isotropic susceptibility case (27).

The magnetic field B_x parallel to $\mathbf{B}_0$ (in the x direction) is the important quantity for determining the influence on T_2*, because B_x influences the spin precession frequency. Often the perturbation of the magnetic field is expressed as $E = (B_x - B_0)/B_0$, which is the same as the fractional shift of the Larmor frequency in the MR signal (18). The fractional frequency shift is

$$E = \frac{\chi}{4}(1-w)\left[\ln\left(\frac{b}{a}\right) + \cos(ka)(\mathrm{Ci}(kb) - \mathrm{Ci}(ka)) - \sin(ka)(\mathrm{Si}(kb) - \mathrm{Si}(ka))\right] \quad r < a \quad [16]$$

$$E = \frac{\chi}{4}\Bigg\{w(1 - \cos(k(r-a))) + (1-w)\left[\ln\left(\frac{b}{r}\right) + \cos(ka)(\mathrm{Ci}(kb) - \mathrm{Ci}(kr)) - \sin(ka)(\mathrm{Si}(kb) - \mathrm{Si}(kr))\right] + \cos(2\theta)\left[w\cos(k(r-a)) + \frac{1-w}{2} + \frac{1+w}{2}\left(-\frac{k^2a^2-2}{k^2r^2} - \frac{2}{kr}\sin(k(r-a)) - \frac{2}{k^2r^2}\cos(k(r-a))\right)\right]\Bigg\} \quad a < r < b \quad [17]$$

$$E = \frac{\chi}{4}\left(\frac{1+w}{2}\right)\left(\frac{b^2-a^2}{r^2}\right)\cos(2\theta) \quad r > b. \quad [18]$$

Inside the axon ($r < a$) the frequency shift is uniform, but it is not zero as it was for the isotropic case (27). If there are many layers of myelin ($n \gg 1$), so that the spacing between adjacent myelin layers is smaller than any other distance scales in the problem,[2] then $E \approx \frac{\chi}{4}(1-w)\ln\left(\frac{b}{a}\right)$. Outside the axon ($r > b$), the frequency shift is nearly the same as for the isotropic case, $E = \frac{\chi}{4}\left(\frac{b^2-a^2}{r^2}\right)\cos(2\theta)$, with the only difference being the factor of $\left(\frac{1+w}{2}\right)$. The factor $\cos(2\theta)$ implies that the frequency shift varies depending on the myelin orientation with respect to $\mathbf{B}_0$. In the myelin sheath ($a < r < b$) the frequency shift oscillates between the myelin and water layers. In the limit of many layers, the frequency shift becomes

$$E = \frac{\chi}{4}\Bigg\{w(1 - \cos(k(r-a))) + (1-w)\ln\left(\frac{b}{r}\right) + \cos(2\theta)\left[w\cos(k(r-a)) + \frac{1-w}{2} - \frac{1+w}{2}\left(\frac{a^2}{r^2}\right)\right]\Bigg\}. \quad [19]$$

In the water-filled spaces between myelin layers we can set $\cos[k(r-a)] = 1$, and Eq. [19] reduces to

$$E = \frac{\chi}{4}\left\{(1-w)\ln\left(\frac{b}{r}\right) + \left(\frac{1+w}{2}\right)\cos(2\theta)\left[1 - \frac{a^2}{r^2}\right]\right\} \quad a < r < b. \quad [20]$$

The factor of $\cos(2\theta)$ implies that the frequency shift is different along the applied magnetic field ($\theta = 0$, 180°) and perpendicular to it ($\theta = 90°$, 270°). The structure of the myelin domain also influences the magnetic field outside the axon. Near the outer surface of the axon, the magnetic field heterogeneity is as large as in the myelin.

Figure 1(a) shows the magnetic field as a function of position within and surrounding the axon, for the case of isotropic susceptibility ($w = 1$). The applied magnetic field is horizontal, and the plot is of $(B_x - B_0)/(B_0\chi)$. The magnetic field oscillations are most apparent where the myelin layers run parallel to the applied magnetic field (90° and 270°), and the oscillations disappear where the myelin layers lie perpendicular to it (0° and 180°). The white stripes (where the magnetic field is largest) correspond to layers of myelin, whereas the dark stripes (where the magnetic field is smaller) correspond to water between myelin layers. If just water protons are imaged, the heterogeneity is somewhat less dramatic than it appears visually in Figure 1 because we assume that there is no water in the regions corresponding to the lipid layers.

The calculation in Figure 1 uses an inner radius of $a = 0.250\ \mu$m and an outer radius of $b = 0.362\ \mu$m, typical of white matter (31). If the myelin repeat distance is $0.016\ \mu$m, this results in $n = 7$. This value of n is smaller than in our previous publication (27), which was more appropriate for a large peripheral nerve.

Figure 1(b), (c) shows $(B_x - B_0)/(B_0\chi)$ for the cases of $w = 0.9$ and $w = 1.1$, corresponding to anisotropic myelin susceptibility. When the magnitude of the susceptibility is higher in the r direction, w is less than unity (Fig. 1(b)); when it is higher in the θ and z directions, w is greater than unity (Fig. 1(c)). The spatial distribution is similar (but not identical) in all three figures. The effect is larger for larger values of w. The case of $w = 0.9$ (Fig. 1(b)) is most biologically relevant. This figure in fact exaggerates the influence of tissue anisotropy. If the magnitude of the susceptibility is of the order of 10×10^{-6} and the magnitude of the difference between the myelin susceptibility in the two directions is about 0.2×10^{-6} (21,28), then the value of w should be of the order of 0.98. We chose values of w over a wider range to more clearly indicate the influence of anisotropy. Figure 1(d) is a plot of the difference between the plots in Figure 1(a) ($w = 1$) and (b) ($w = 0.9$). The difference is only a few percent in water-filled regions.

[2]This implies that both $k(b-a) \gg 1$ and $ka \gg 1$.

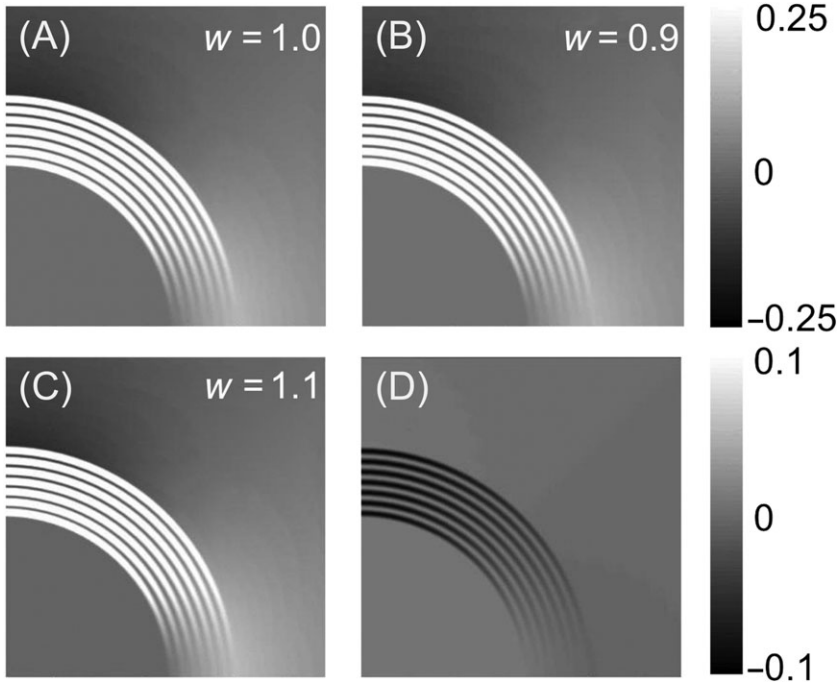

Figure 1. (a)–(c) The dimensionless quantity $(B_x - B_0)/(B_0\chi)$ as a function of position in and around a myelinated axon, calculated using Eqs [16]–[18], for the isotropic case ($w = 1$) (a) and anisotropic cases $w = 0.9$ (b) and $w = 1.1$ (c). The applied magnetic field is horizontal. (d) A plot of the difference between the $w = 0.9$ and 1.0 cases. In (a)–(c) the color bar (which ranges from −0.25 to 0.25) is saturated; the value of $(B_x - B_0)/(B_0\chi)$ is approximately unity at its peak within the myelin. (d) uses the color bar that ranges from −0.1 to 0.1. Each panel shows an area of 0.5 by 0.5 μm. The plots are symmetric, so only one quadrant of the axon is shown. $a = 0.25$ μm, $b = 0.362$ μm, $n = 7$.

Case 2. The applied magnetic field is parallel to the axon

The magnetic field parallel to the axon ($\mathbf{B}_0 = B_0\mathbf{k}$) is a trivial case where we can find an exact solution. All equations are satisfied and boundary conditions are met if $\mathbf{B} = \frac{\mu_z}{\mu_0}\mathbf{B}_0$, where μ_z is equal to μ_0 inside and outside the axon, and is given by Eq. [2] in the myelin. Therefore, the magnetic field varies throughout the myelin sheath, but in the regions of water between myelin layers ($\cos(k(r-a)) \approx 1$) the magnetic field is simply the applied field B_0, implying that the fractional frequency shift is zero and the myelin susceptibility should not contribute to T_2* (13).

DISCUSSION

We calculate the magnetic field in and around a myelinated axon in the presence of an applied magnetic field, accounting for the anisotropic magnetic susceptibility of the myelin, and find an analytical solution that predicts how the magnetic field depends on the model parameters. When the magnetic field is applied perpendicular to the axon, (1) the magnetic field in the intracellular space is influenced by the myelin when the myelin is anisotropic; (2) the magnetic field in the myelin sheath oscillates between the lipid and water layers; and in the water layer the magnetic field is heterogeneous; and (3) the magnetic field in the extracellular space outside the myelin sheath ($r > b$) is heterogeneous. In all regions, the heterogeneous distribution of Larmor frequencies causes the spins to dephase, shortening T_2*. If the magnetic field is along the axon, the magnetic field is homogeneous within water-filled regions, the spins do not dephase, and the magnetic susceptibility has no effect on T_2*.

Figure 1 shows a significant heterogeneity of the magnetic field, but the plots for different values of w are similar to each other. This result suggests that the underlying myelin structure is the primary source of heterogeneity leading to changes in T_2*, and that the myelin anisotropy contribution is relatively small. In addition, our results indicate that the magnetic field is heterogeneous in both the myelin-water layers and the extracellular space. Because the total amount of water in the extracellular space should be much larger than the amount of myelin water (because there are no lipids there taking up much of the volume), the T_2* value may be determined as much by water outside surrounding the axon as it is by water trapped between myelin layers.

If water can diffuse into the myelin, it will sense a different magnetic field than in the region between myelin layers, and will therefore experience a larger frequency shift (21,32). This effect is present both when the axon is perpendicular to the applied magnetic field and when the axon is parallel to the magnetic field. It is also present if protons in the lipids rather than in water are imaged.

In general a magnetic field $\mathbf{B}_0$ applied at an angle α with respect to the z axis can be decomposed into a component parallel to the axon, $B_0 \cos\alpha$, and a component perpendicular to the axon, $B_0 \sin\alpha$. The perturbation of the magnetic field experienced by the water will be zero parallel to the axon and will be proportional to $B_0 \sin\alpha$ perpendicular to the axon. When this perturbation is projected onto the direction of the applied magnetic field and then divided by B_0, the result is the fractional Larmor frequency shift given in Eqs [16]–[18] multiplied by $\sin^2\alpha$. This argument for the $\sin^2\alpha$ dependence is very general, and does not depend on our particular myelin model. It applies to models with other myelin distributions as well, such as that in

Reference 21. Note that θ and α are very different quantities: θ is the microscopic directional dependence of the Larmor shift that would be averaged over in an MR signal from a voxel containing many axons, while α is the macroscopic angle between the magnetic field and the local axonal fiber axis.

One interesting conclusion of our model is that "anisotropy" arises from two sources. The cylindrical shape of the axons implies that the effect of the myelin susceptibility is different for a magnetic field along or across the axon (the $\sin^2\alpha$ dependence). Therefore, the T_2* value should depend on the direction of the magnetic field. This effect is present even when the susceptibility is isotropic ($w = 1$). The anisotropy of the myelin itself affects the magnitude of the perturbation, but it does not affect the $\sin^2\alpha$ dependence on the direction of the applied field. In other words, myelin anisotropy is very different from anisotropy arising from the structure of axons, and one must be careful to differentiate between various meanings of the term (21).

Our results indicate a marked oscillation in the frequency shift experienced in the myelin. The use of a uniform susceptibility for the entire myelin sheath results in an average magnetic field within the sheath, but ignores the heterogeneity within the myelin where the water between myelin layers experiences a different magnetic field than the lipids within the myelin. The oscillating nature of the susceptibility distribution is crucial for predicting the heterogeneity.

We model the permeability of the myelin as a sinusoidal function. Sukstanskii and Yablonskiy represented it as a piecewise constant function (21). The two analyses provide similar results: the intracellular frequency shift is non-zero only if the myelin is anisotropic, the extracellular frequency shift varies as $\cos(2\theta)/r^2$, and the expressions for the frequency shift in the water between myelin layers have similar, although not identical, forms. It is not obvious to us which approximation is closer to reality: a piecewise constant permeability or a sinusoidal one. Electron density curves from x-ray diffraction studies (see Fig. 4–3 in Reference 33) suggest that the structure of myelin is intermediate between these two extremes. Having both solutions implies that those results the two models have in common are more likely to be independent of the details of the permeability distribution. Their expressions require either taking sums over the n layers of myelin or replacing those sums as integrals (a reasonable but not exact approximation). Our expressions are a closed-form analytical solution of our model correct to first order in the small parameter χ that contain no sums, but do contain the relatively unfamiliar sine and cosine integral functions. Both models highlight the difference between the anisotropy of the lipids layers and the "anisotropy" arising from the cylindrical microstructure of the axons.

In a subsequent publication (34), Yablonskiy and Sukstanskii extended their model to account for diffusion of water between myelin and intermyelin layers. In this case, there is a significant difference between our model and theirs. Because our model postulates a continuous sinusoidal permeability distribution, the predicted frequency shift will change continuously between myelin and water, as opposed to the discontinuous jump when going from myelin to water in the piecewise continuous model by Yablonskiy and Sukstanskii. This means that water cannot experience a dramatically different frequency shift by diffusing only a very small distance from a pure water pool to a pure lipid environment (their "hip-hop" mechanism (34)). For a significant effect, water would need to diffuse a significant fraction of the thickness of one myelin layer.

Our model is based on several assumptions.

- We consider only a single axon, but a nerve bundle or fascicle typically consists of many axons. A more detailed study is needed to predict the magnetic field perturbation in and around a closely spaced pack of axons, accounting for interactions between and among them.
- Our solution includes only terms first order in χ; we neglect terms proportional to χ^2 or higher powers. Because $|\chi|$ is of the order of 10^{-5}, this approximation should be very accurate.
- We assume that water layers between the myelin correspond to $\cos(k(r-a)) = 1$. However, the aqueous region extends over regions where the cosine has values less than unity. To completely characterize the effect of the heterogeneity, one should integrate over the water-filled region.
- We calculate the macroscopic magnetic field, but to determine the microscopic field that individual spins experience we need to apply the Lorentz sphere (21,35). However, when we calculate the frequency shift relative to the frequency at a large radius in the extracellular space, E, the Lorentz sphere correction will — at least to first order in χ — cancel out in the intracellular space, in the extracellular space, and in the water layers corresponding to $\cos(k(r-a)) \approx 1$. Only when one uses our model to obtain the frequency shift within the myelin lipid layers, $\cos(k(r-a)) \approx -1$, will the Lorentz sphere correction be required to obtain the correct frequency shift, but in that case we assume that there is no water to image.
- We assume that the susceptibility oscillates sinusoidally across the myelin sheath. Our assumption of a sinusoidal dependence can be thought of as the first term in a Fourier series representation of the susceptibility distribution, and we expect that it captures the first-order behavior resulting from a spatially oscillating susceptibility. Details such as unequal widths of the lipid and water layers in myelin (21), or alternating thick and thin layers (33), would require higher-order terms in the Fourier series.
- We assume that the axon is long and straight, has a circular cross-section, and does not undulate, splay, twist, or bend. We believe that this is a good approximation over short distances. There are also nodes of Ranvier punctuating long lengths of myelin insulation in these axons. Those nodes should have a negligible effect on the microscopic variation of the magnetic field because they appear rarely: approximately once every 100 axon diameters (36). Homogenization methods could be used to account for the nodes, using techniques such as those proposed by Burridge and Keller (37), and used by Basser (38) in a composite model of myelinated axons.
- We assume that the magnetic susceptibility is anisotropic, with different values parallel to the fatty acid chains in the lipids and perpendicular to them (18,20,21).
- Finally, we ignore other factors that may contribute to signal heterogeneity, such as water existing within the lipid layers, the contribution of protons in the lipids themselves, the chemical shift, perturbations caused by blood vessels, differences in diffusion, the chemical exchange of protons between water and macromolecules, etc. Diffusion may be a particularly important issue, as the magnetic field in the myelin is heterogeneous over small length scales, where diffusion may occur rapidly, and over distances that are short considering the diffusion time of these experiments (21). A crucial

question is if myelin susceptibility contributes more or less than these other factors to a reduction in T_2*.

Our results (and those in Reference 21) predict that the magnetic field heterogeneity will be different depending on the angle α between the magnetic field and the long axis of the nerve fiber. It will be zero when $\alpha = 0$ and greatest when $\alpha = 90°$, and this heterogeneity should vary as $\sin(2\alpha)$. These results are consistent with experimental data (22–26). However, even though our model includes myelin anisotropy, it does not predict a $\sin(4\alpha)$ contribution to the angular dependence of the magnetic field heterogeneity, which is consistent with Reference 26 but inconsistent with References 23 and 25. Note, however, that under some conditions the relaxation time constant may depend on the square of the magnetic field heterogeneity, implying the possibility that T_2* could have a $\sin(4\alpha)$ component (39).

Detailed experimental confirmation of this model will be difficult, because the heterogeneity of the magnetic field occurs over distances that are small compared with the voxel size used in MRI. One option would be to build a phantom scaled up by perhaps a factor of 1000 or more. With such a model we could resolve a heterogeneous frequency shift from susceptibility differences, but other phenomena such as diffusion effects may not scale properly.

This work hints at the enormous complexity of modeling the magnetic resonance signal arising within and around white matter pathways in the central nervous system (CNS) or nerve tracts in the peripheral nervous system (PNS). A key challenge is not just incorporating composition, material properties, morphology, and heterogeneous and anisotropic susceptibility *per se*, but incorporating them at the relevant length scales (40). White matter has a fractal-like structure consisting of bundles of microtubules and neurofilaments within the intraaxonal space at nanometer length scales surrounded by a lipid membrane and concentric myelin-water layers whose anisotropy appears to arise from the molecular arrangement of radially oriented long chain fatty acids — from both their terminal amine group and the alkanes themselves. At coarser length scales, individual axons form packs, these packs form fascicles, and these fascicles are bundled together to form white matter pathways in the CNS or nerve bundles in the PNS at a centimeter length scale. Capturing the salient magnetic field perturbations caused by composition, morphology, heterogeneity, and anisotropy at length scales spanning more than eight orders of magnitude, ranging from molecule to organ dimensions, presents a profound conceptual challenge. Even modeling the magnetic resonance signal at the cubic millimeter voxel length scale is an extremely complex task. Moreover, the measured MRI phase used to infer features of magnetic susceptibility is itself subject to experimental artifacts, such as RF and physiological noise, small- and large-scale motion, and image distortion, to name a few. Taken together, the use of acquired MRI phase signals to infer specific features of axons or nerves using susceptibility effects is a complicated and potentially ill-posed inverse problem.

Acknowledgments

This research was supported by the National Institutes of Health grant R01EB008421 (BJR, SP), and by the Intramural Research Program of the Eunice Kennedy Shriver National Institute of Child Health and Human Development (PJB). We thank the anonymous reviewers for their valuable contributions.

REFERENCES

1. MacKay A, Whittall K, Adler J, Li D, Paty D, Graeb D. *In vivo* visualization of myelin water in brain by magnetic resonance. Magn. Reson. Med. 1994; 31: 673–677.
2. Meyers SM, Laule C, Vavasour IM, Kolind SH, Madler B, Tam R, Traboulsee AL, Lee J, Li DKB, MacKay AL. Reproducibility of myelin water fraction analysis: a comparison of region of interest and voxel-based analysis methods. Magn. Reson. Imaging 2009; 27: 1096–1103.
3. Kolind SH, Madler B, Fischer S, Li DKB, MacKay AL. Myelin water imaging: implementation and development at 3.0 T and comparison to 1.5 T measurements. Magn. Reson. Med. 2009; 62: 106–115.
4. Deoni SCL, Mercure E, Blasi A, Gasston D, Thomson A, Johnson M. Mapping infant brain myelination with magnetic resonance imaging. J. Neurosci. 2011; 31: 784–791.
5. Kitzler HH, Su J, Zeineh M, Harper-Little C, Leung A, Kremenchutzky M, Deoni SC, Rutt BK. Deficient MWF mapping in multiple sclerosis using 3D whole-brain multi-component relaxation MRI. NeuroImage 2012; 59: 2670–2677.
6. Kozlowski P, Liu J, Yung AC, Tetzlaff W. High-resolution myelin water measurements in rat spinal cord. Magn. Reson. Med. 2008; 59: 796–802.
7. Deoni SCL, Zinkstok JR, Daly E, Ecker C, MRC AIMS Consortium, Williams SCR, Murphy DGM. White-matter relaxation time and myelin water fraction differences in young adults with autism. Psychol. Med. 2015; 45: 795–805.
8. Deoni SCL, Dean DC, III, O'Muircheartaigh J, Dirks H, Jerskey BA. Investigating white matter development in infancy and early childhood using myelin water fraction and relaxation time mapping. NeuroImage 2012; 63: 1038–1053.
9. Dean DC, III, O'Muircheartaigh J, Dirks H, Waskiewicz N, Lehman K, Walker L, Han M, Deoni SCL. Modeling healthy male white matter and myelin development: 3 through 60 months of age. NeuroImage 2014; 84: 742–752.
10. Haacke EM, Reichenbach JR. *Susceptibility Weighted Imaging in MRI*. Wiley: Hoboken, NJ, 2011.
11. Haacke EM, Liu S, Buch S, Zheng W, Wu D, Ye Y. Quantitative susceptibility mapping: current status and future directions. Magn. Reson. Imaging 2015; 33: 1–15.
12. Haacke EM, Mittal S, Wu Z, Neelavalli J, Cheng Y-CN. Susceptibility-weighted imaging: technical aspects and clinical applications, Part 1. Am. J. Neuroradiol. 2009; 30: 19–30.
13. He X, Yablonskiy DA. Biophysical mechanisms of phase contrast in gradient echo MRI. Proc. Natl. Acad. Sci. U. S. A. 2009; 106: 13558–13563.
14. Li W, Wu B, Liu C. Quantitative susceptibility mapping of human brain reflects spatial variation in tissue composition. NeuroImage 2011; 55: 1645–1656.
15. Liu C. Susceptibility tensor imaging. Magn. Reson. Med. 2010; 63: 1471–1477.
16. Özarslan E, Basser PJ. Dependence of the MR lineshape for white-matter on the orientation of the B_0 field: insights from a three-phase model. In *11th International Conference on Magnetic Resonance Microscopy*. China University of Petroleum: Beijing, 2011; 173.
17. Li W, Wu B, Avram AV, Liu C. Magnetic susceptibility anisotropy of human brain *in vivo* and its molecular underpinnings. NeuroImage 2012; 59: 2088–2097.
18. Wharton S, Bowtell R. Fiber orientation-dependent white matter contrast in gradient echo MRI. Proc. Natl. Acad. Sci. U. S. A. 2012; 109: 18559–18564.
19. Wharton S, Bowtell R. Effects of white matter microstructure on phase and susceptibility maps. Magn. Reson. Med. 2015; 73: 1258–1269.
20. Sati P, van Gelderen P, Silva AC, Reich DS, Merkle H, Zwart JA, Duyn JH. Micro-compartment specific T_2* relaxation in the brain. NeuroImage 2013; 77: 268–278.
21. Sukstanskii A, Yablonskiy DA. On the role of neuronal magnetic susceptibility and structure symmetry on gradient echo MR signal formation. Magn. Reson. Med. 2014; 71: 345–353.
22. Denk C, Hernandez Torres E, MacKay A, Rauscher A. The influence of white matter fibre orientation on MR signal phase and decay. NMR Biomed. 2011; 24: 246–252.
23. Lee J, van Gelderen P, Kuo L-W, Merkle H, Silva AC, Duyn JH. T_2*-based fiber orientation mapping. NeuroImage 2011; 57: 225–234.

24. Sati P, Silva AC, van Gelderen P, Gaitan MI, Wohler JE, Jacobson S, Duyn JH, Reich DS. In vivo quantification of T_2* anisotropy in white matter fibers in marmoset monkeys. NeuroImage 2012; 59: 979–985.
25. Oh S-H, Kim Y-B, Cho Z-H, Lee J. Origin of B_0 orientation dependent R_2* (=1/T_2*) in white matter. NeuroImage 2013; 73: 71–79.
26. Rudko DA, Martyn Klassen L, de Chickera SN, Gati JS, Dekaban GA, Menon RS. Origins of R_2* orientation dependence in gray and white matter, Proc. Proc. Natl. Acad. Sci. U. S. A. 2014; 111: E159–E167.
27. Roth BJ, Puwal S, Basser PJ. Local magnetic field perturbations caused by magnetic susceptibility heterogeneity in myelin-water layers within an axon. J. Coupled Syst. Multiscale Dyn. 2015; 3: 228–232.
28. Lounila J, Ala-Korpela M, Jokisaari J, Savolainen MJ, Kesaniemi YA. Effects of orientational order and particle size on the NMR line positions of lipoproteins. Phys. Rev. Lett. 1994; 72: 4049–4052.
29. Jackson JD. *Classical Electrodynamics*, 3rd edn. Wiley: New York, 1999.
30. Abramowitz M, Stegun IA. *Handbook of Mathematical Functions With Formulas, Graphs, and Mathematical Tables*. Dover: New York, 1965.
31. Liewald D, Miller R, Logothetis N, Wagner H-J, Schuz A. Distribution of axon diameters in cortical white matter: an electron-microscopic study on three human brains and a macaque. Biol. Cybern. 2014; 108: 541–557.
32. Duyn JH. Frequency shifts in the myelin water compartment. Magn. Reson. Med. 2014; 71: 1953–1955.
33. Morell P, Quarles RH. Myelin formation, structure and biochemistry. In *Basic Neurochemistry: Molecular, Cellular and Medical Aspects*, Siegel GJ (ed), 6th edn. Lippincott Williams and Wilkins: Philadelphia, PA, 1999, pp. 69–93.
34. Yablonskiy DA, Sukstanskii AL. Biophysical mechanisms of myelin-induced water frequency shifts. Magn. Reson. Med. 2014; 71: 1956–1958.
35. Durrant CJ, Hertzberg MP, Kuchel PW. Magnetic susceptibility: further insights into macroscopic and microscopic fields and the sphere of Lorentz. Magn. Reson. Annu. 2003; 18: 72–95.
36. Rushton WAH. A theory of the effects of fibre size in medullated nerve. J. Physiol. 1951; 115: 101–122.
37. Burridge R, Keller J. Poroelasticity equations derived from microstructure. J. Acoust. Soc. Am. 1981; 70: 1140–1146.
38. Basser PJ. Cable equation for a myelinated axon derived from its microstructure. Med. Biol. Eng. Comput. 1993; 31: S87–S92.
39. Yablonskiy DA, Haacke EM. Theory of NMR signal behavior in magnetically inhomogeneous tissues: the static dephasing regime. Magn. Reson. Med. 1994; 32: 749–763.
40. Edwards J, Daniel E, Kinney J, Bartol T, Sejnowski T, Harris D, Johnston K, Bajaj C, VolRover N. Automated reconstruction of cellular morphology for multiscale dynamical simulation of neural activity. Neuroinformatics 2014; 12: 277–289.